Experimental studies on flow visualization and velocity field of compression ramp with different incoming boundary layers*

Wu Yu(武 宇), Yi Shi-He(易仕和), He Lin(何 霖)†, Chen Zhi(陈 植), and Zhu Yang-Zhu(朱杨柱)

College of Aerospace Science and Engineering, National University of Defense Technology, Changsha 410073, *China*

(Received 27 March 2014; revised manuscript received 27 April 2014; published online 24 September 2014)

Experimental studies which focus on flow visualization and the velocity field of a supersonic laminar/turbulent flow over a compression ramp were carried out in a Mach 3.0 wind tunnel. Fine flow structures and velocity field structures were obtained via NPLS (nanoparticle-tracer planar laser scattering) and PIV (particle image velocimetry) techniques, time-averaged flow structures were researched, and spatiotemporal evolutions of transient flow structures were analyzed. The flow visualization results indicated that when the ramp angles were 25°, a typical separation occurred in the laminar flow, some typical flow structures such as shock induced by the boundary layer, separation shock, reversed flow and reattachment shock were visible clearly. While a certain extent separation occurred in turbulent flow, the separation region was much smaller. When the ramp angles were 28°, laminar flow separated further, and the separation region expanded evidently, flow structures in the separation region were complex. While a typical separation occurred in turbulent flow, reversed flow structures were significant, flow structures in the separation region were relatively simple. The experimental results of velocity field were corresponding to flow visualization, and the velocity field structures of both compression ramp flows agreed with the flow structures well. There were three layered structures in the U component velocity, and the V component velocity appeared like an oblique "v". Some differences between these two compression ramp flows can be observed in the velocity profiles of the shear layer and the shearing intensity.

Keywords: compression ramp, incoming boundary layer, fine flow structure, velocity field

PACS: 47.32.Ef, 47.80.Jk, 47.80.Cb, 47.54.De **DOI:** 10.1088/1674-1056/23/11/114702

1. Introduction

In supersonic flow, separation and shock wave boundary layer interaction caused by a compression ramp will result in a complicated flow field, as illustrated in Fig. 1. The low frequency motion of shock may lead to wall pressure oscillations; the shock wave boundary layer interactions are important origins of aerodynamic drag, which can cause fluctuations of aerodynamic force and deteriorate the performance of aircrafts. Therefore, experimental studies of flow structures in a compression ramp are necessary for the optimization of aerodynamic design.

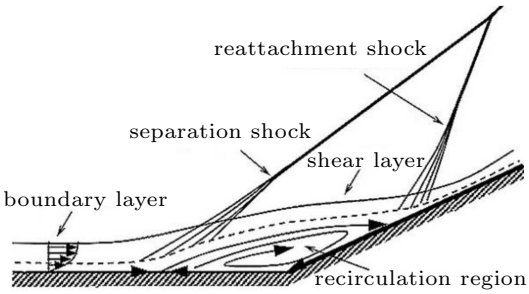


Fig. 1. Sketch of compression ramp flow field.

In the past few decades, a lot of numerical simulations and experimental researches focusing on compression ramp flow have been carried out. Some numerical methods such as DNS (direct numerical simulation),[1] LES (large-eddy simulation),[2] and LES/RANS (large-eddy simulation/Reynolds-averaged Navier-Stokes)[3] were applied in computations, the mean and fluctuating characteristics have been researched, and the large-scale unsteady motion of shock foot and three-dimensional streamwise structures were found. However, the influence of different incoming boundary layers on flow structures was not illustrated clearly by numerical simulations.

Lee and Wang[4] performed experiments to research hypersonic turbulent flow over a number of compression corner models, the results showed that coherent structures existed in the incoming boundary layer and separated flow region, and the shock oscillation was probably caused by coherent structures in the separated region. An experiment had been carried out by Settles *et al.*[5] to detail the influence that was produced by different deflection angles, and the characteristics of corresponding flow fields were described. Smits *et al.*[6] used hot-wires to measure the longitudinal mass-flux fluctuations and the mass-weighted turbulent shear stress in compression ramp flows under different deflection angles. Based on PLMS (planar laser Mie scattering), Chan *et al.*[7] researched the detailed structures of the incoming boundary layer and separation shock in a Mach 5 compression ramp; the results suggested that the incoming boundary layer was comprised of large-scale vortex structures, and the low-frequency motion of the shock foot was related to the thickness of the undisturbed bound-

*Project supported by the National Natural Science Foundation of China (Grant Nos. 11172326 and 11302256).

†Corresponding author. E-mail: helin.101sys@gmail.com

© 2014 Chinese Physical Society and IOP Publishing Ltd

ary layer. A pulsed-plasma jet actuator[8] was used to control the unsteadiness of separation shock in a Mach 3 compression ramp; HSPIV (high-speed particle image velocimetry)[9] was applied to research the low-frequency dynamics characteristics of the separation region. Zheltovodov[10] reviewed some of the recent progress of compression ramps, and also proposed some perspectives and problems for future study.

Although the aforementioned experiments relate to many aspects of compression ramp flow such as the flow structure, wall pressure measurement, flow control, and so on, there are few studies which focus on the influence of different incoming boundary layers, especially on fine flow structures, as the previous experiment data have low resolutions. Traditional flow visualization techniques such as schlieren and shadow are confronted with the weakness of low spatial resolution, while PLMS, PLIF (planar laser induced fluorescence), and FRS (filtered Rayleigh scattering) encounter the problems of weak scattering signals or low signal-to-noise ratios, and are not suitable for measurement in a supersonic flow that requires high spatiotemporal resolution. NPLS (nanoparticle-tracer planar laser scattering) is a flow visualization technique which was developed by Yi and Zhao[11,12] for measuring fine structures in supersonic flow. Its spatial resolution achieves micrometer scale, with a time resolution of 6 ns, the temporal correlation resolution reaches 0.2 μs. In some previous experiments[13–18] NPLS technique has been applied very well.

In this paper, fine flow structures and velocity field structures of compression ramps with laminar and turbulent incoming boundary layers under 25° and 28° ramp angles are obtained via NPLS and PIV (particle image velocimetry) techniques. The spatiotemporal evolutions of flow field and the time-averaged flow structures are analyzed, some different characteristics of these two compression ramp flows in flow separations and flow field structure are compared and discussed.

2. Experimental facility

2.1. Supersonic wind tunnel

All experiments were carried out in a Mach 3.0 wind tunnel. To eliminate disturbances, the wind tunnel was directly connected, and the nozzle, which was designed based on a B-spline curve, ran in an indraft mode. The incoming flow was dried and dust free, the total pressure and stagnation temperature were $P_0 = 0.1$ MPa and $T_0 = 300$ K, and the unit Reynolds number was $Re = 7.5 \times 10^6$ m^{-1}, and the diffuser was connected to a vacuum chamber downstream. As shown in Fig. 2, the cross section of the test chamber was 100 mm × 120 mm, the two side faces with 250 mm × 120 mm dimensions were installed with optical glass for imaging and measuring.

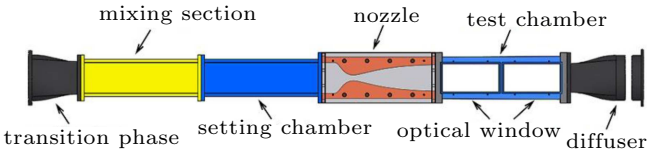


Fig. 2. (color online) Mach 3.0 wind tunnel.

2.2. NPLS testing system

NPLS technique is a planar laser scattering for measuring fine flow structure based on nanoparticles for tracing. With excellent following ability of nanoparticles, the complicated structures in the flow field can be revealed exactly by the distribution of scattering light. The particle used in this paper is TiO_2 with a nominal diameter of 18 nm; a shock wave response test was performed in a previous study[12] to measure the particle size, and the results indicated that the diameter of the particle is 42.5 nm. The particle response time, which is measured by a shock wave response test, is $\tau_p = 250$ ns, the thickness of the turbulent boundary layer measured by PIV is $\delta_{0.99} = 8.0$ mm, the main stream speed is $U_\infty = 622.5$ m·s^{-1}, therefore, the characteristic flow time is $\tau_f = \delta_{0.99}/U_\infty = 12.85$ μs, and the Stokes number $S_t = \tau_p/\tau_f = 0.019 < 0.05$. It can be inferred that the nanoparticles used in this paper are appropriate for NPLS and PIV measurements.

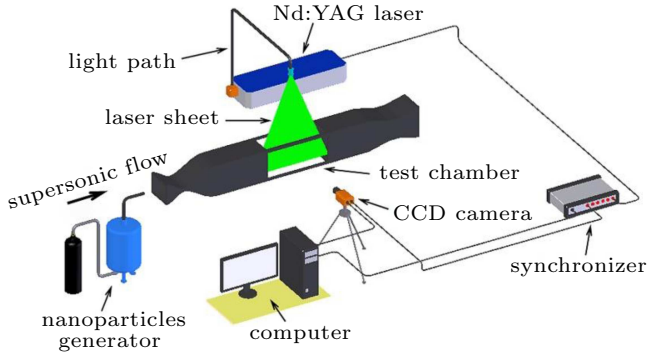


Fig. 3. (color online) NPLS system.

As shown in Fig. 3, the NPLS system is composed of a light source, synchronous controller, imaging, data acquisition and processing components and nanoparticles generator. A dual-cavity Nd:YAG pulsed laser, which emits two laser beams of 532-nm wavelength and 6-ns pulse width, is used as the light source, and a light sheet of less than 1 mm illuminates the interested regions through the optical lens. An interline transfer double-exposure CCD camera whose resolution is 2 k × 2 k is used for taking images and its shortest double-exposure interval is 0.2 μs. The synchronizer, which has an accuracy of 250 ps, ensures the laser and the CCD work simultaneously. The computer is in charge of transmitting instructions, gathering, storing and processing images. More details about NPLS system can be found in the previous study.[12]

2.3. Compression ramp models

The test models include laminar flow (model I) and turbulent flow (model II), each one of them has an adjusting device to make the ramp angle variable. The compression ramp models are shown in Fig. 4.

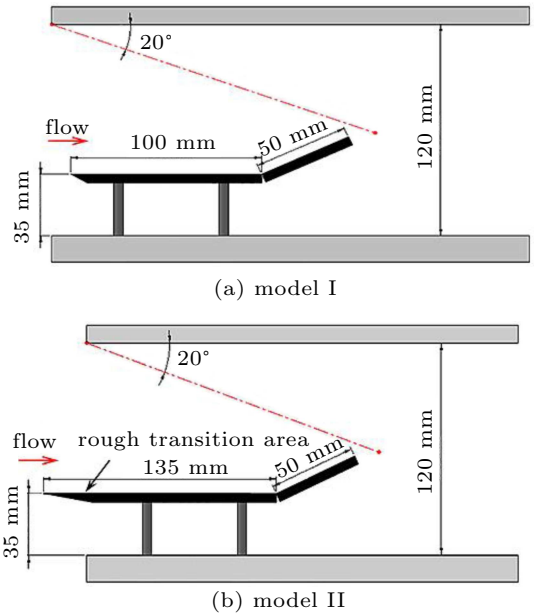


Fig. 4. (color online) Sketch of compression ramp models. (a) Laminar flow model; (b) turbulent flow model.

By changing the roughness of the upstream wall surface, laminar and turbulent boundary layers can be formed. Model I is located in the main stream area, a laminar incoming boundary layer is formed by supersonic flow; model II is also located in the main stream area, while a rough transition region on the upstream wall surface makes the incoming boundary layer turbulent flow.

In model I, the length of the flat wall is $l_1 = 100$ mm, the length of the ramp is $s_1 = 50$ mm, and the distance between the surface of the flat wall and the bottom of the test chamber is $h_1 = 35$ mm; in model II, the length of the flat wall is $l_2 = 135$ mm, the length of the ramp is $s_2 = 50$ mm, and the distance between the surface of the flat wall and the bottom of the test chamber is $h_2 = 35$ mm. The spanwise widths of the two models are $d_1 = d_2 = 100$ mm, which are the same as the spanwise size of the test chamber and enable the flow to be considered as two-dimensional. It can be seen from Fig. 4 that the theoretical angles of Mach wave induced by fixing step are 20° due to the reasonable locations of models when experiments are carried out, the Mach wave does not disturb the testing region.

3. Visualization and analysis of fine flow structures

3.1. Transient flow structures

Because of the different values of wall roughness, there are obvious differences between the incoming boundary layers of the two test models.

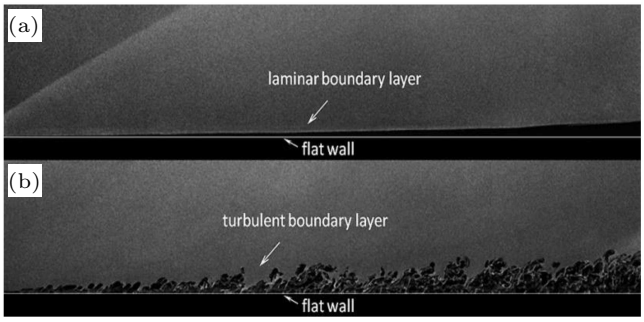


Fig. 5. NPLS image of incoming boundary layers. (a) Mode I; (b) model II.

Figure 5 shows different incoming boundary layers of the two test models. The incoming boundary layer of model I is a laminar flow, it develops slowly and there is no structure in the boundary layer. The incoming boundary layer of model II, which increases constantly in the streamwise direction, is a turbulent flow; it is much thicker than the laminar boundary layer, and there are some coherent structures.

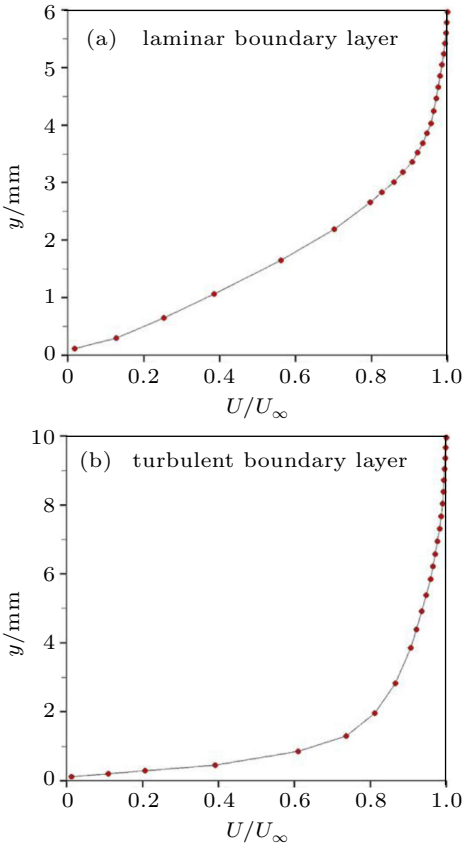


Fig. 6. (color online) Velocity profiles of incoming boundary layers (the location is $X = -65$ mm). (a) Laminar boundary layer; (b) turbulent boundary layer.

In order to obtain the velocity profiles of upstream undisturbed boundary layers accurately, a PIV experiment in a small local region is carried out. The deflection point of the model is selected as the origin, and the exact streamwise location of the velocity profile of the boundary layer is $X = -65$ mm. Velocity profiles of upstream undisturbed boundary layers are

provided in Fig. 6. It can be seen clearly that the boundary layer in model I is a typical laminar flow, the boundary layer in model II is a turbulent flow, which is not fully developed. As a result, the velocity profile of the turbulent boundary layer is less full.

Transient flow structures of the two models are shown in Figs. 7 and 8, which have distinctly revealed the structures of flow field and the evolutions, all the origins are located at the deflection point.

Figure 7 shows transient flow structures of 25° compression ramp models. The laminar boundary layer in model I develops and converts to a turbulent flow rapidly under the influence of the adverse pressure gradient, at the same time, a shock is induced. Based on the analysis of a large number of transient flow fields, it can be found that the induced shock is related to the fast development of the boundary layer. Flow separation occurs at somewhere upstream of the deflection point, and a separation region appears. A sheer layer is formed between the separated flow and the reverse flow a series of compression waves that are induced by large scale vortices, which are located at the external area of the separation region, and separation shock is formed as a result of the convergence of compression waves. Flow reattachment occurs on the ramp and reattachment shock is formed; the boundary layer after reattachment redevelops with structural evolutions.

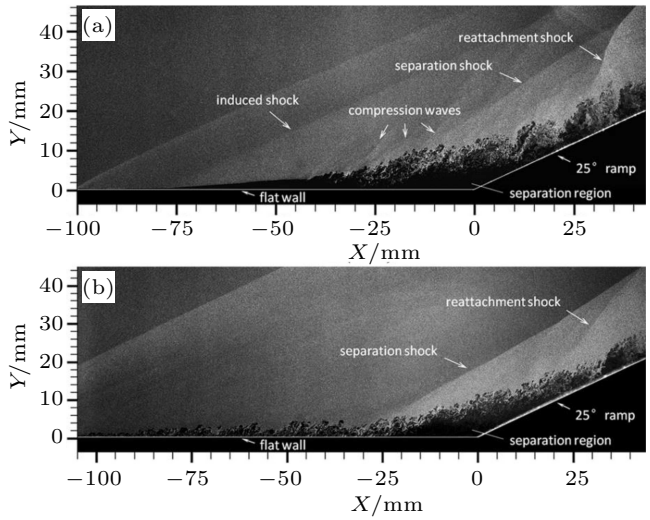


Fig. 7. Transient flow structures of 25° compression ramps. (a) Model I; (b) model II.

For model II, flow structures are obviously different. Firstly, the turbulent boundary layer, which shows structural irregularities and fluctuations, is much thicker than the laminar boundary layer; it contrasts with the developing process of the laminar boundary layer, which includes instability and transition. Secondly, a typical flow separation occurs in model I with the 25° ramp angle, while a certain extent flow separation occurs in model II under the same ramp angle. The range of separation region in model II is smaller, there is no induced shock caused by the development of the boundary layer, compression waves also do not appear, and a sharp separation shock is visible with flow separation, while the reattachment shock is much weaker.

Figure 8 shows transient flow structures of 28° compression ramp models. It can be seen that with the increase of ramp angles, the laminar flow separates further in model I. As a result, a laminar boundary layer develops more rapidly, the transition position moves upstream, and the separation region expands significantly. The induced shock and separation shock move upstream, and the reattachment shock moves downstream: the flow structures in the separation region are very complicated.

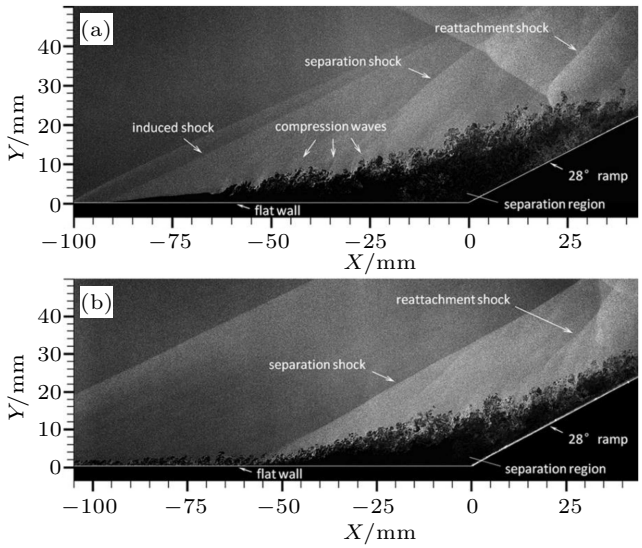


Fig. 8. Transient flow structures of 28° compression ramps. (a) Model I; (b) model II.

By contrast, a typical flow separation occurs in model II. The shear layer, separation shock, the recirculation region and reattachment shock can be identified clearly from the image. With regard to the flow field, no induced shock caused by the development of a boundary layer can be seen. At the end of the separation region, a series of compression waves converge to be reattachment shock. Reattachment occurs somewhere on the ramp, and the turbulent boundary layer after reattachment is much thicker than the upstream boundary layer: the flow structures in the separation region are relatively simple.

3.2. Time-averaged flow structures

A time-averaged flow field can be obtained by performing an averaging process to hundreds of transient flow fields. Although some transient characteristics are erased, the disturbances caused by instabilities are also eliminated, which is advantageous to analyze the time-averaged structural characteristics. Time-averaged flow fields based on 400 transient flow fields are shown in Figs. 9 and 10.

As shown in Fig. 9, when the ramp angles are 25°, the laminar boundary layer in model I develops at an angle of 4.8°, and the turbulent boundary layer in model II develops at an angle of 33°. Structures such as the boundary layer, shock and so on can be identified by the analysis of image gray level and

Canny edge detection.[15] Results show that in model I, the angle between induced shock and the flat wall is 23.1°, the angle between separation shock and the flat wall is 38.3°, and that between the reattachment shock and the ramp is 32.7°. The turbulent boundary layer after reattachment increases at an angle of 3.6°. In model II, the angle between separation shock and the flat wall is 27.8°, the angle between reattachment shock and the ramp is 17.5°. The turbulent boundary layer after reattachment increases at an angle of 3.1°.

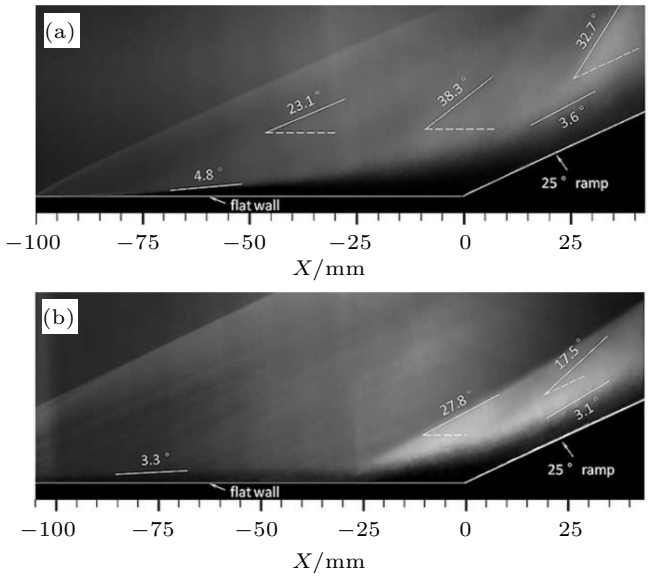


Fig. 9. Time-averaged flow fields of 25° compression ramps. (a) Model I; (b) model II.

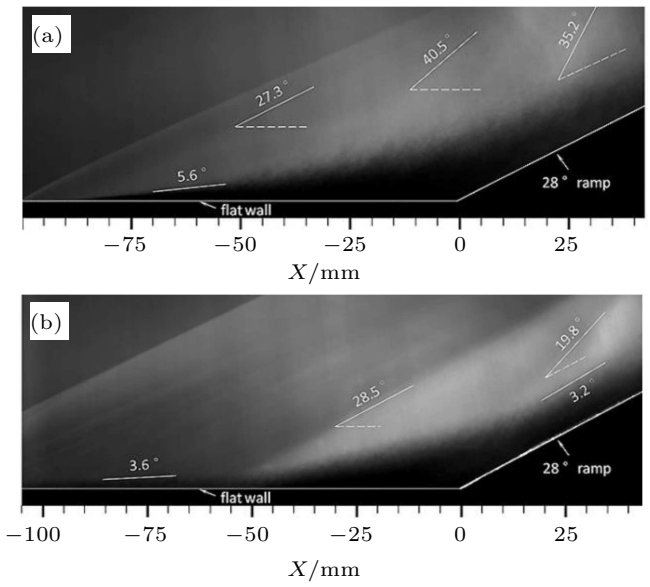


Fig. 10. Time-averaged flow fields of 28° compression ramps. (a) Model I; (b) model II.

It can be seen in Fig. 10 that when the ramp angles are 28°, the laminar boundary layer in model I develops at an angle of 5.6°, and the turbulent boundary layer in model II develops at an angle of 36°. Measurements show that in model I, the angle between induced shock and the flat wall is 27.3°, the angle between separation shock and the flat wall is 40.5°, and that between reattachment shock and the ramp is 35.2°. In model II, the angle between separation shock and the flat wall is 28.5°, the angle between reattachment shock and the ramp is 19.8° and the turbulent boundary layer after reattachment increases at an angle of 3.2°.

3.3. Time-evolutions of flow structures

According to the flow visualization results, two typical flow statuses including model I 25° and model II 28° are selected to analyze time-evolution characteristics.

Figure 11 provides time-evolutions of flow structures in model I with 25° ramp angle; the time interval between the two images is 10 μs. Structure "A" at t is the state of the boundary layer when it changes from a laminar flow into a vortex, after 10 μs it becomes structure "a" at t and moves downstream about 4.6 mm. Compared with "A", "a" represents structural expansion and shear deformation because of flow separation, which illustrates that coherent structures in the laminar boundary layer have the properties of low speed and significant deformation. Structures "B" and "C" locate at the external area of the boundary layer, in the same time interval, they move downstream about 5.0 mm. At the same time, "b" and "c" have represented structural incline and stretching deformation. By comparing with each other, it can be seen from the two images that compression waves have movements as large scale vortices in the boundary layer move, which illustrates that the compression waves have an inseparable relationship with the large vortices in the boundary layer.

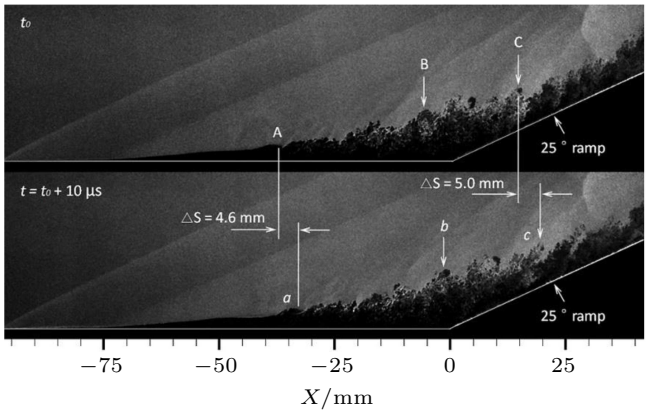


Fig. 11. Time-evolutions of flow structures in model I.

Figure 12 provides time-evolutions of flow structures in model II with a 28° ramp angle; the time interval between the two images is 10 μs. "A" at t_0 is a large scale structure in the turbulent boundary layer, after 10 μs it becomes structure "a", which is accompanied with a certain extent deformation and moves downstream about 5.6 mm. It can be inferred that coherent structures in the turbulent boundary layer have less deformation and higher speed than those in the laminar boundary layer. "B" and "C" at t_0 are the large scale structures, which

locate at the external region of the boundary layer. Compared to "*b*" and "*c*" after 10 μs, it is obvious that with the influence of separation and reattachment shock, the speed of coherent structures decreases, and in the same time interval, they move downstream about 4.6 mm. Moreover, "*b*" and "*c*" have shown structural incline, for which there are two main reasons: firstly, the viscosity in the near wall region and the influence of an adverse pressure gradient; secondly, the reversed flow and the shearing effect.

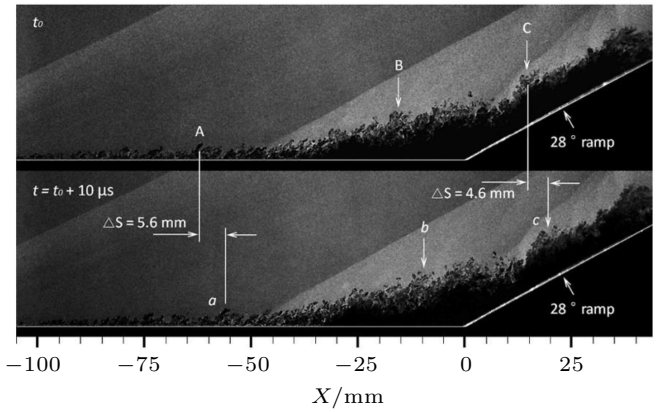


Fig. 12. Time-evolutions of flow structures in model II.

What is worth noticing is that the variations of image gray level after separation shock in model II are more remarkable than that in model I, which means that the density changes in model II are more significant and the separation shock is stronger when the incoming boundary layer is a turbulent flow.

4. Measurement and analysis of velocity field structures

4.1. Velocity field structures in the separation region

Complicated structures can be found in separation regions, which are revealed not only in flow visualization, but also in the velocity field.

Mean velocity field structures of separation regions with 25° ramp angles are shown in Fig. 13. In model I, a typical separation of laminar flow occurs with the influence of an adverse pressure gradient. The speed of air flow decreases and the flow direction changes under the effects of separation and reattachment shock Flow separation and reattachment are revealed distinctly by streamlines, a recirculation zone including reversed flow is created by separation and the velocity profiles of the shear layer are formed gradually. Low speed reverse flow structures exist in the region covered by the shear layer. Velocity distributions in the main stream area are homogeneous.

In model II, a certain extent separation of turbulent flow occurs. The effects of separation shock are well revealed by streamlines, while the recirculation zone is much smaller. A shear layer is formed after turbulent flow separates, although its range is small, the shearing effect is intenser than the laminar shear layer, and the velocity gradients caused by the shearing effect in the whole recirculation zone are relatively large. Shear layer structures increase constantly as the flow develops downstream.

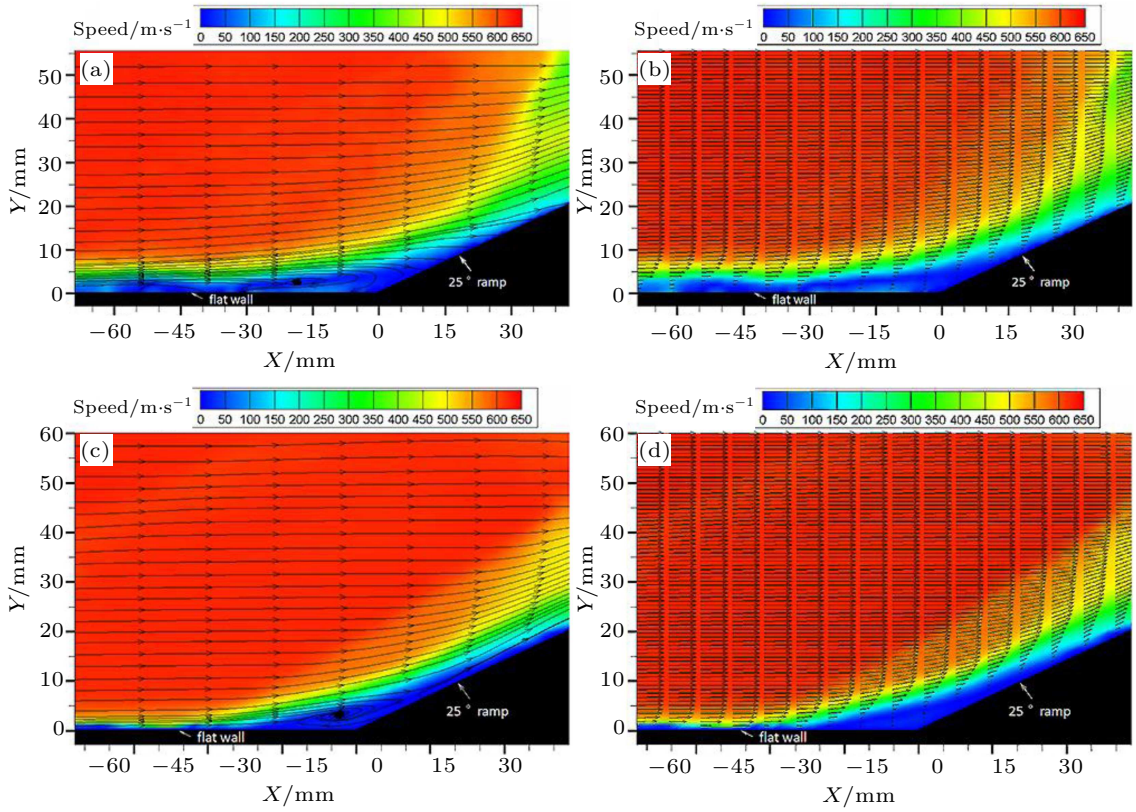


Fig. 13. (color online) Streamlines (left) and vectors (right) of mean velocity fields in separation regions of 25° ramps. (a) and (b) Model I, (c) and (d) model II.

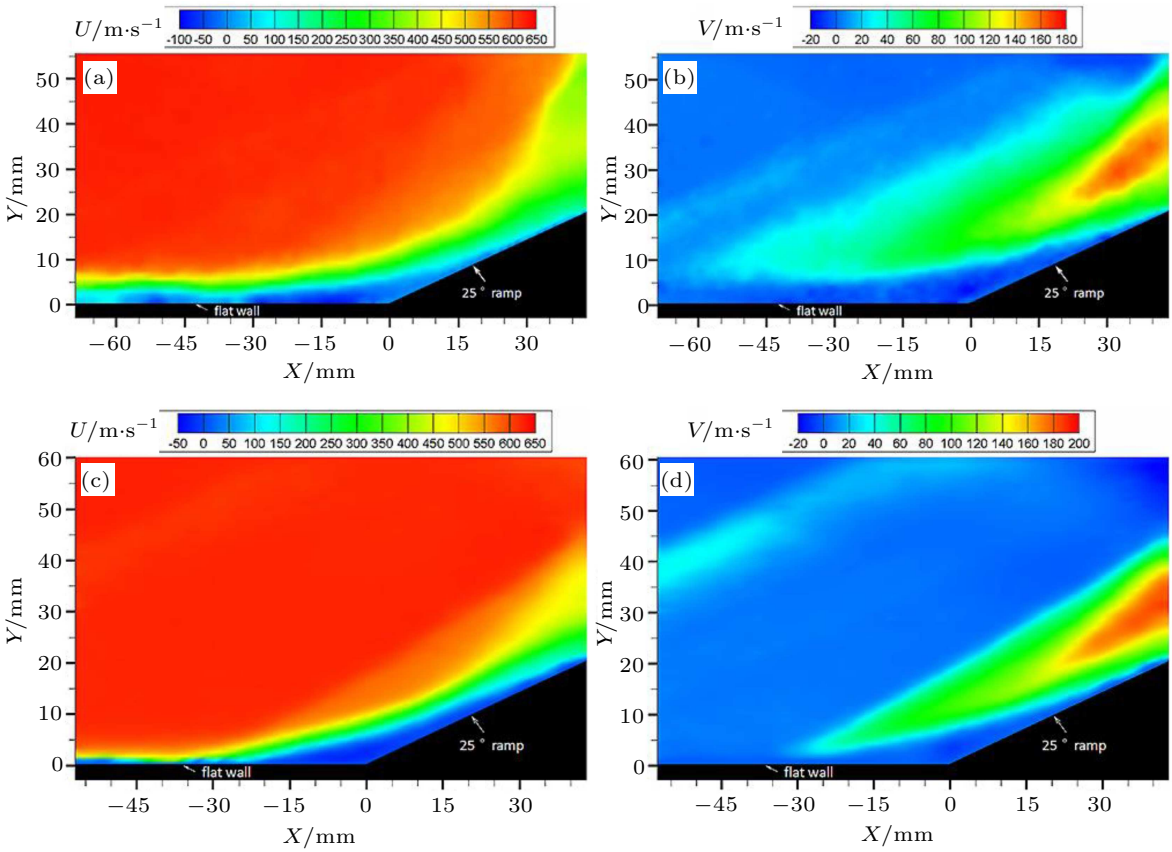


Fig. 14. (color online) Mean velocity charts of U (left) and V (right) components in separation regions of 25° ramps. (a) and (b) Model I, (c) and (d) model II.

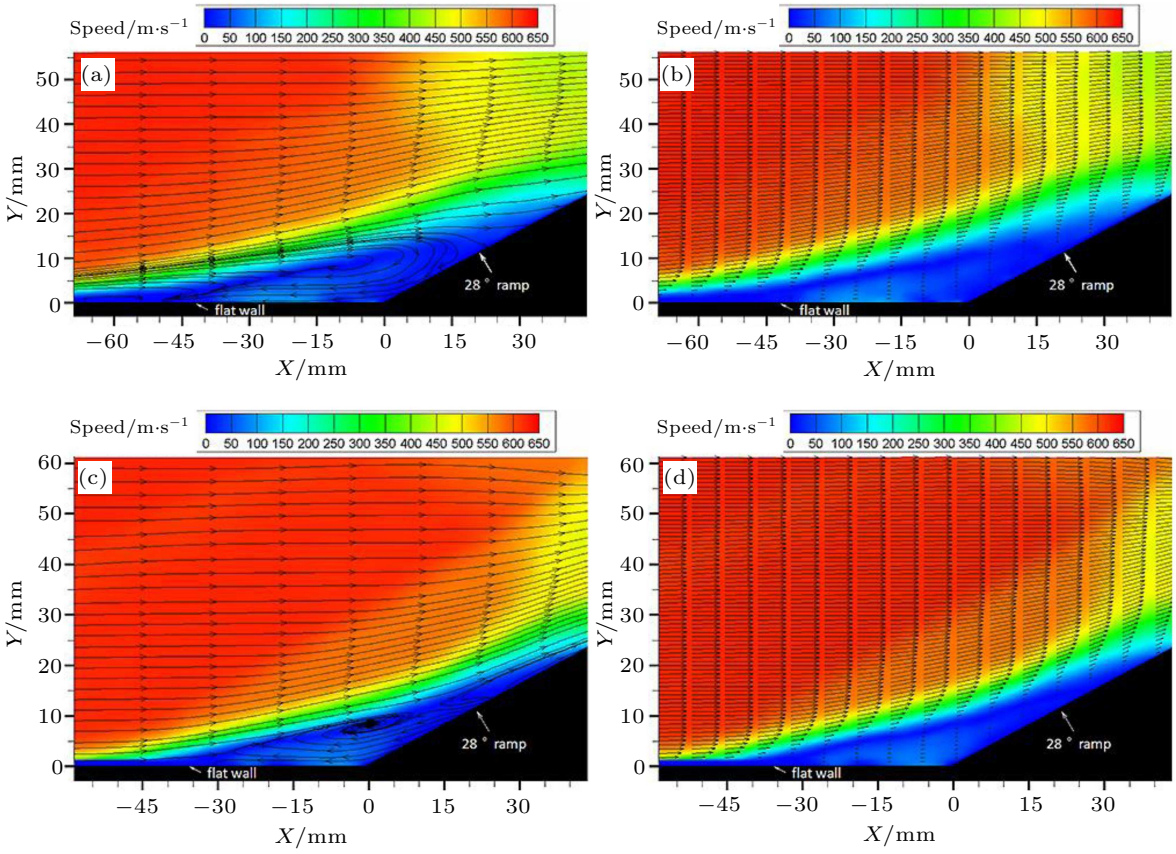


Fig. 15. (color online) Streamlines (left) and vectors (right) of mean velocity fields in separation regions of 28° ramps. (a) and (b) Model I, (c) and (d) model II.

Figure 14 shows the mean velocity distributions of U and V components in 25° ramps. According to the results, it can be seen that in model I, the main features of U component velocity are velocity shear and gradient variations, three layered structures including main stream area, shear layer, and recirculation zone are significant. It is interesting that the V component velocity looks like an oblique "v" above the ramp. There is a recirculation zone near the ramp, where the velocity is lower than that in the shear layer; as a result, the bottom boundary of an oblique "v" is formed. Due to flow channel contraction caused by the ramp, there is acceleration along the vertical direction in the main stream area. As the flow channel contracted further, the V component velocity increases further; finally, a local region where the V component velocity is highest appears. Afterwards, the V component velocity decreases gradually under the influence of separation shock, and the upper boundary of the oblique "v", which is composed of disturbance area and separation shock, is formed.

In model II, it can be seen from the mean velocity charts of the U component velocity that there is a significant boundary between reverse flow structures and the shear layer: the recirculation zone, which is covered by the shear layer, undertakes the upstream turbulent boundary layer as a real interface. The characteristics of V component velocity are similar to those in model I, while the oblique "v" in model II is smaller, narrower and closer to the downstream region, which is corresponding to characteristics of the velocity distribution in the separation region.

Mean velocity field structures of separation regions with 28° ramp angles are shown in Fig. 15. As ramp angles increase, the changes of velocity field structures are remarkable. In model I, the separation region expands distinctly, reverse flow structures, which are revealed by streamlines, are more significant, and the reattachment point moves downstream. Flow structures in the separation region are so complex that it is difficult to distinguish separation shock and reattachment shock. The shear layer increases somewhat and the intensity of the shearing effect is stronger, as a result, the velocity gradients in the recirculation zone become larger.

In model II, a typical flow separation can be seen from the results, while the range of reversed flow is still smaller than that in model I. Separation shock and reattachment shock can be identified clearly according to the mean velocity field structures, flow separation and reattachment are revealed distinctly by streamlines, at the same time, the influence of compression waves has been expressed by the changes of velocity vectors at the end of the recirculation zone. Although the turbulent shear layer is smaller than the laminar shear layer, its shearing intensity is more intense, even though at the end of the recirculation zone, the velocity gradients are still large.

Figure 16 shows mean velocity distributions of U and V components in 28° ramps. In model I, it can be seen clearly from the charts that three layered structures in U component velocity are more significant and the growth of the shear layer is faster. The V component velocity is still like an oblique "v", compared with the status of 25° ramp, the oblique "v" expands significantly and moves upstream, which agrees with the characteristics of the flow structures in the 28° ramp very well.

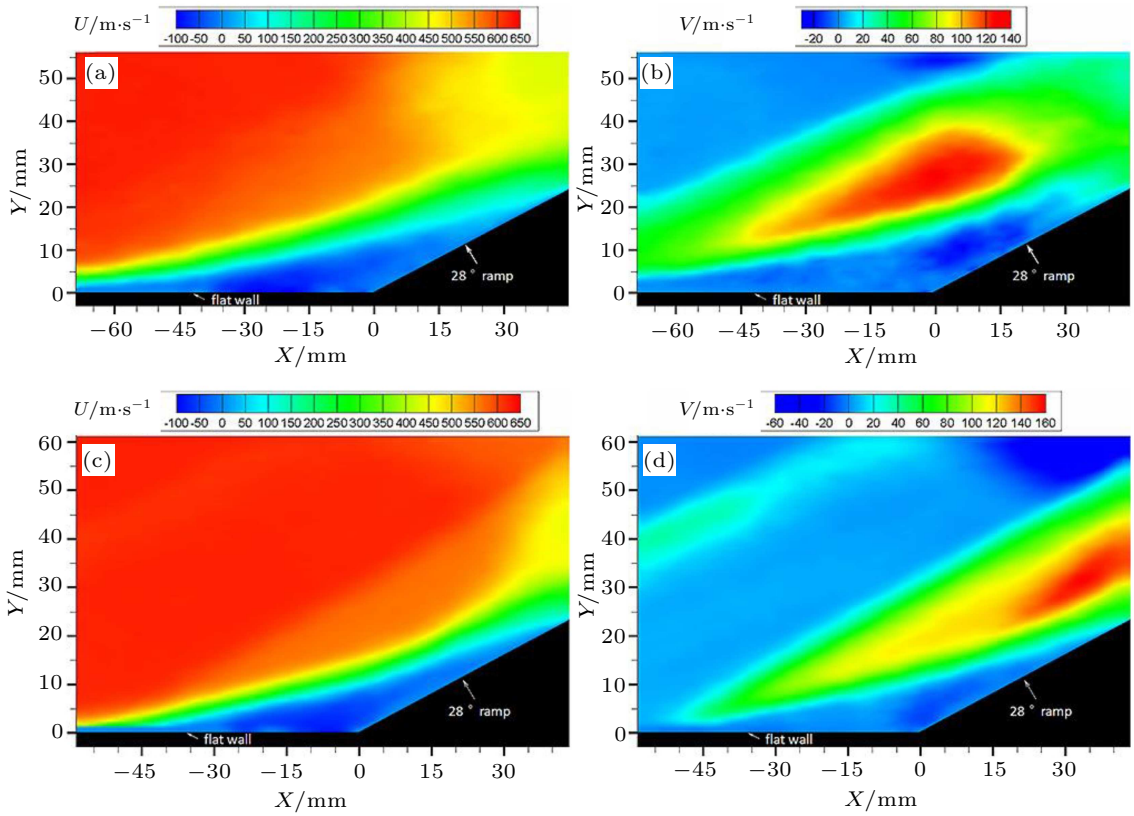


Fig. 16. (color online) Mean velocity charts of U (left) and V (right) components in separation regions of 28° ramps. (a) and (b) Model I, (c) and (d) model II.

In model II, there are still three layered structures in U component velocity, separation shock and reattachment shock can be identified clearly, and the influence of compression waves, which locate at the end of the recirculation zone, is expressed distinctly from the charts. The main characteristics of V component velocity are similar to that in model I, while the oblique "v" in model II is longer and narrower.

4.2. Velocity field structures in the vicinity of the separation point

Mean velocity field structures in the vicinity of the separation point with 25° ramp angles are provided in Fig. 17. According to the results, in model I, the streamwise speed of the laminar boundary layer changes slowly, the velocity profiles are not full, and the velocity gradient variations are small,

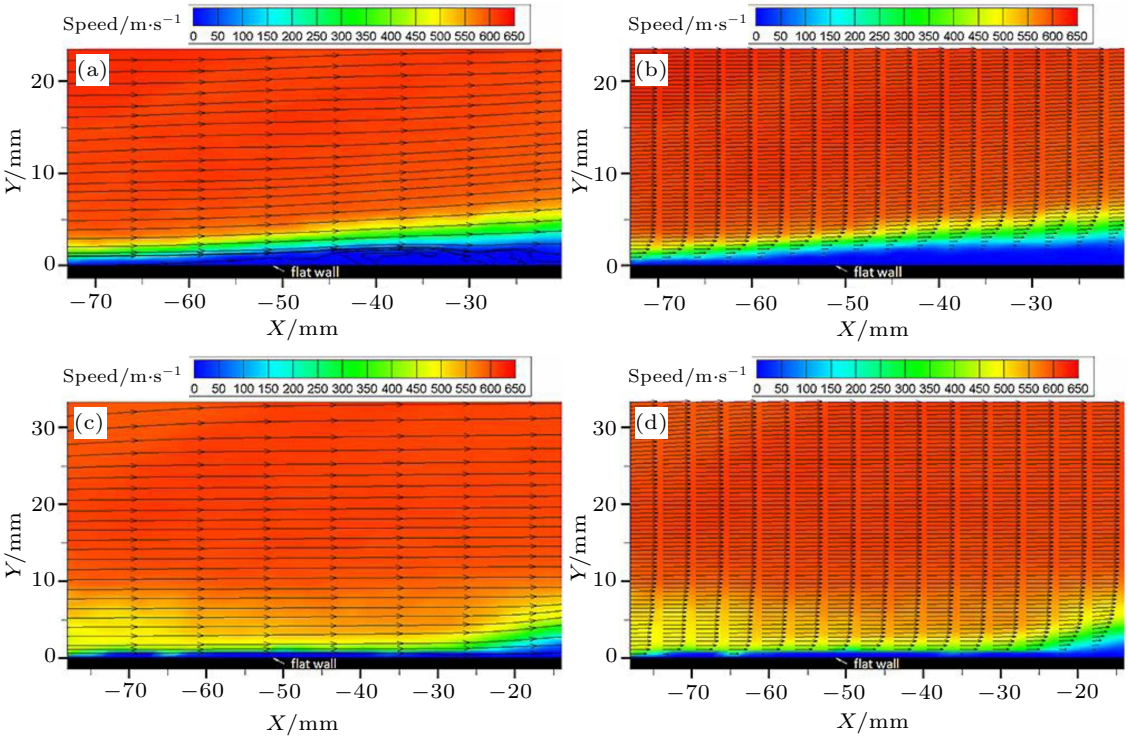


Fig. 17. (color online) Streamlines (left) and vectors (right) in the vicinity of the separation point in 25° ramps. (a) and (b) Model I, (c) and (d) model II.

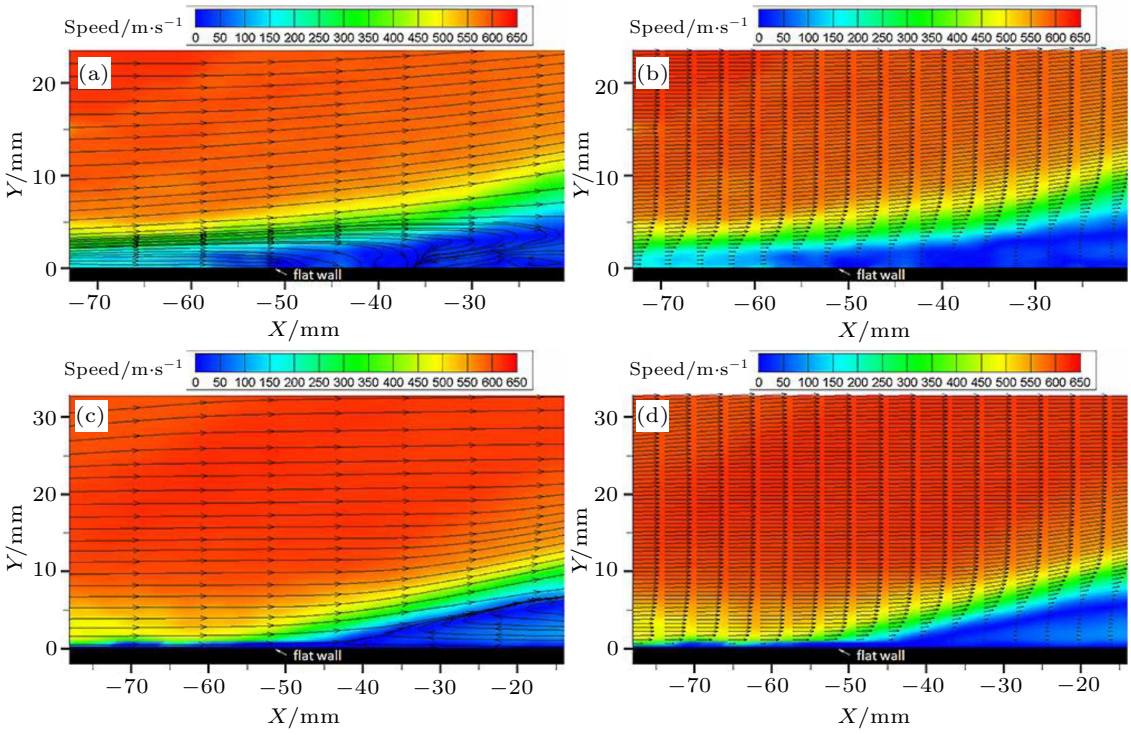


Fig. 18. (color online) Streamlines (left) and vectors (right) in the vicinity of the separation point in 28° ramps. (a) and (b) Model I, (c) and (d) model II.

which are the typical characteristics of the laminar boundary layer. The speed of the main stream area is about 620 m/s, and the velocity distributions are homogeneous. The movements of reversed flow are revealed by streamlines, which indicate that flow separation has occurred in this region, and the variations of velocity vectors reveal the growth of the shear layer.

In model II, the streamwise speed of the turbulent boundary layer changes irregularly because of its structural irregularity, the velocity profiles are relatively full, and large velocity gradients exist along the vertical direction, which are the typical characteristics of the turbulent boundary layer. It can be inferred from the velocity charts that the speed in the main stream area is about 620 m/s, the speed in the boundary layer increases rapidly to hundreds of meters per-second in a short distance along the vertical direction, and the boundary-layer flow is formed. The trend of streamlines indicates that there is no reverse flow structure, and the velocity vectors reveal that the shear layer starts to increase.

Mean velocity field structures in the vicinity of the separation point with 28° ramp angles are provided in Fig. 18. On the basis of velocity distributions, in model I, the movements of reversed flow have become more prominent with comparison to the status of the 25° ramp, the recirculation zone expands significantly, and the growth of the shear layer becomes more rapid.

In model II, reverse flow structures are revealed distinctly by streamlines, which indicates that flow separation has occurred in this region. Velocity profiles of the turbulent boundary layer become less full gradually under the influence of flow separation, variations of velocity vectors show that shear layer structures and shearing intensity increase constantly.

4.3. Velocity field structures in the vicinity of reattachment point

Mean velocity field structures in the vicinity of the reattachment point with 25° ramp angles are provided in Fig. 19. In model I, flow structures are continuous with those in the separation region, reverse flow structures and reattachment, which occurs on the ramp, are well revealed by streamlines. The range of the recirculation zone decreases constantly, while the mixing layer structures, which approach to the ramp gradually, become remarkable. The range of the shear layer increases gradually, the reattachment point locates at the end of the recirculation zone.

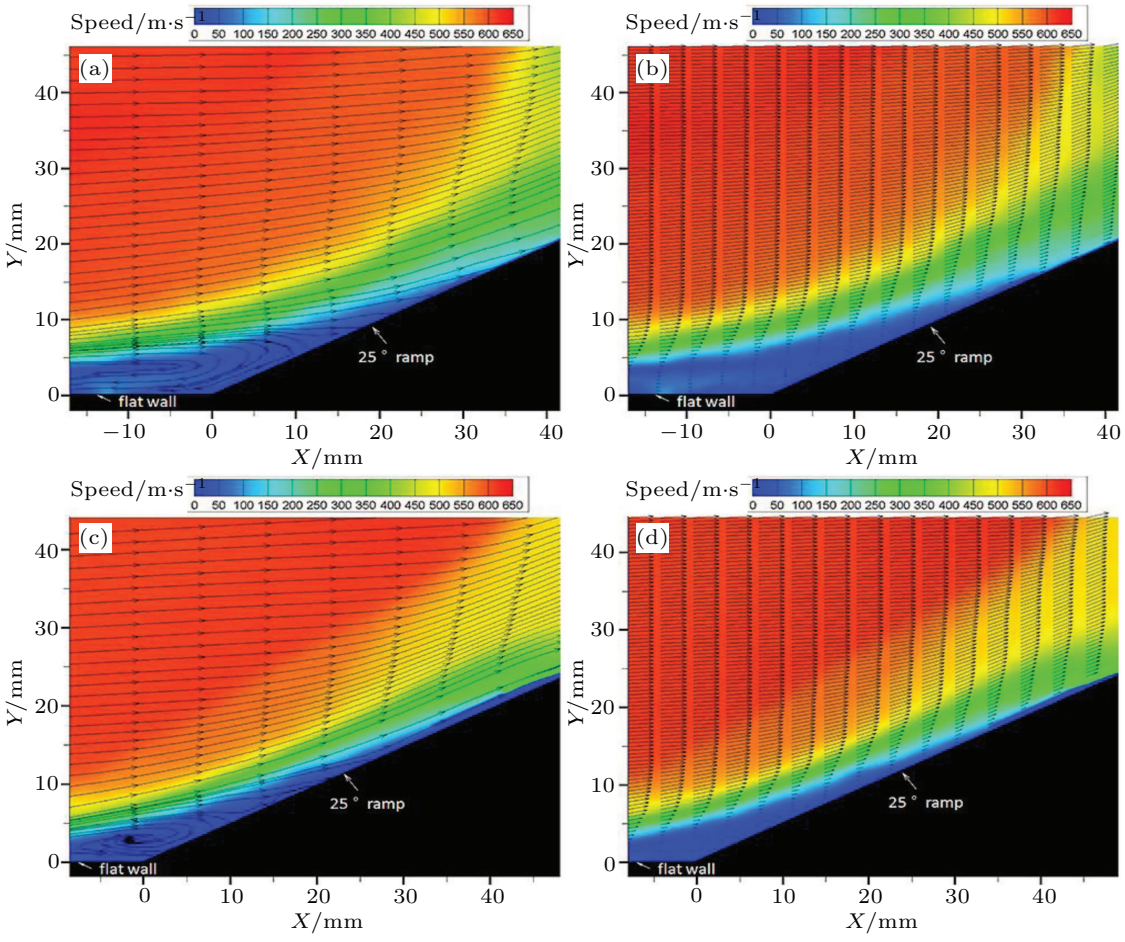


Fig. 19. (color online) Streamlines (left) and vectors (right) in the vicinity of the reattachment point in 25° ramps. (a) and (b) Model I, (c) and (d) model II.

In model II, the separation region is smaller than that in model I, localized reversed flow movements are visible by streamlines. The flow direction of the main stream changes distinctly under the influence of reattachment shock, the turbulent shear layer approaches to the ramp gradually, the range of the recirculation zone covered by the shear layer decreases constantly, but velocity gradients in the end of recirculation zone are still very large. The boundary layer redevelops after reattachment and the velocity gradients along the vertical direction increase somewhat. Moreover, the velocity profiles become full again gradually.

With a comprehensive analysis of streamlines and vector variations, it can be concluded that flow reattachment in model I occurs at the location of $X = 15$ mm on the ramp, and in model II, reattachment occurs at the location of $X = 10$ mm on the ramp, where the mean flow speeds near the wall are zero.

Mean velocity field structures in the vicinity of the reattachment point with 28° ramp angles are provided in Fig. 20. It can be seen from the charts that, the recirculation zones in both models expand significantly, the reattachment points move downstream and the growths of shear layers are more remarkable.

With a comprehensive analysis of streamlines and vector variations, it can be concluded that flow reattachment in model I occurs at the location of $X = 25$ mm on the ramp, and in model II, reattachment occurs at the location of $X = 20$ mm on the ramp, where the mean flow speeds near the wall are zero.

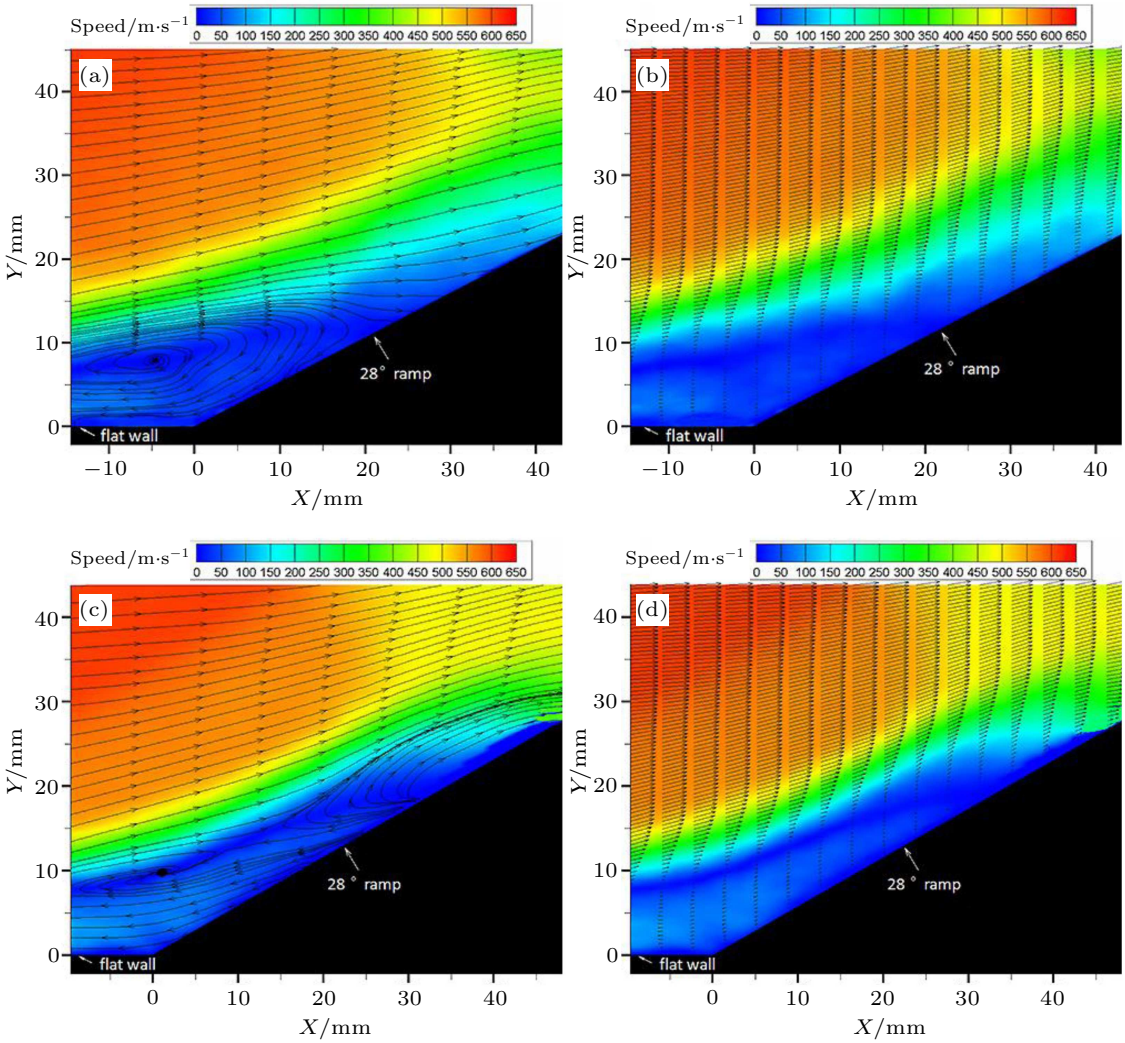


Fig. 20. (color online) Streamlines (left) and vectors (right) in the vicinity of the reattachment point in 28° ramps. (a) and (b) Model I, (c) and (d) model II.

5. Conclusion

In the present paper, experimental studies of compression ramp flows with laminar and turbulent incoming boundary layers are carried out via NPLS and PIV techniques, in which fine flow structures and velocity field structures are obtained. Compared with traditional flow visualization techniques, NPLS can reveal fine structures and spatiotemporal evolutions of a flow field more distinctly.

According to the flow visualization results, it can be concluded that a supersonic laminar flow is instable and prone to separate in the compression ramp; by comparison, because of its structural irregularities and intense fluctuations, supersonic turbulent flow is more stable and difficult to separate. When the ramp angles are 25°, a laminar boundary layer develops and converts to be turbulent flow rapidly, a typical flow separation occurs, and an induced shock caused by the fast development of the laminar boundary layer is visible. At the same time, a series of compression waves, which are induced by large scale structures, converge to be separation shock. While the turbulent boundary layer increases slowly, a certain extent of flow separation occurs, and the separation region is much smaller, there is no induced shock and compression wave in flow field. When the ramp angles are 28°, the separation region of the laminar boundary layer expands significantly as flow separates further, the transition position moves upstream and the boundary layer increases more rapidly: flow structures in the separation region are very complicated. However, a typical flow separation occurs in the turbulent boundary layer, reverse flow structures can be seen clearly in the flow field, and a series of compression waves converge to be reattachment shock at the end of the recirculation zone: flow structures in the separation region are relatively simple.

The velocity field structures agree with the flow visualization results very well, which indicates that compared with laminar flow, turbulent flow is more difficult to separate when it suffers from the influence of an adverse pressure gradient. When the ramp angles are 25°, a recirculation zone is created by the separation of laminar flow, flow separation and reattachment are revealed clearly by streamlines, and the velocity profiles of the shear layer grow gradually. However, the shear layer created by the separation of the turbulent boundary layer is relatively small, and the range of reversed flow, which is revealed by streamlines, is also smaller. While the shearing effect in turbulent flow is intenser, large velocity gradients can be seen in the whole recirculation zone. When the ramp angle is 28°, movements of reversed flow in the laminar boundary layer are more significant, and the reattachment point moves downstream. Although the range of reversed flow in the turbulent boundary layer is still smaller than that in the laminar boundary layer, the shearing intensity is stronger.

In a word, the different performances of laminar flow and turbulent flow in the compression ramp still have inseparable relationships with their own properties, and the differences between them, which are induced by the characteristics of the incoming boundary layer from the upstream region, have been developing in the whole process.

References

[1] Wu M and Martin M P 2007 *AIAA J.* **45** 879
[2] Loginov M S, Adams N A and Zheltovodov A A 2006 *J. Fluid Mech.* **565** 135
[3] Gieseking D A and Edwards J R 2012 *AIAA J.* **50** 2057
[4] Lee C and Wang S 1995 *Exp. Fluids* **19** 143
[5] Settles G S, Fitzpatrick T J and Bogdonoff S M 1979 *AIAA J.* **17** 579
[6] Smits A J and Muck K C 1987 *J. Fluid Mech.* **182** 291
[7] Chan S C, Clemens N T and Dolling D S 1995 *AIAA Paper* 2195
[8] Narayanaswamy V, Raja L and Clemens N 2012 *Phys. Fluids.* **24** 076101
[9] Ganapathisubramani B, Clemens N T and Dolling D S 2009 *J. Fluid Mech.* **636** 397
[10] Zheltovodov A A 2006 *AIAA Paper* 0496
[11] Yi S H, He L, Zhao Y X, Tian L F and Cheng Z Y 2009 *Sci. China* **52** 2001
[12] Zhao Y X, Yi S H, Tian L F, He L and Cheng Z Y 2009 *Sci. China* **52** 3640
[13] He L, Yi S H, Tian L F, Chen Z and Zhu Y Z 2013 *Chin. Phys. B* **22** 24704
[14] Chen Z, Yi S H, He L, Tian L F and Zhu Y Z 2012 *Chin. Sci. Bull.* **57** 584
[15] Wu Y, Yi S H, Chen Z, Zhang Q H and Gang D D 2013 *Acta Phys. Sin.* **62** 184702 (in Chinese)
[16] Zhu Y Z, Yi S H, Chen Z, Ge Y, Wang X H and Fu J 2013 *Acta Phys. Sin.* **62** 084219 (in Chinese)
[17] Zhang Q H, Yi S H, Zhu Y Z, Chen Z and Wu Y 2013 *Chin. Phys. Lett.* **30** 044701
[18] Zhu Y Z, Yi S H, He L, Tian L F and Zhou Y W 2013 *Chin. Phys. B* **22** 014702